JOURNAL OF THE KOREAN ASTRONOMICAL SOCIETY
29: S295 ~ S298, 1996

SPECTRAL DIAGNOSTICS OF THE ENERGETIC PARTICLES IN SOLAR FLARES

C. FANG,[1] M. D. DING,[1] J. C. HENOUX,[2] AND W. Q. GAN[3]
[1]Department of Astronomy, Nanjing University, Nanjing, China
[2]Observatoire de Paris, DASOP URS326, Meudon, 92195, France
[3]Purple Mountain Observatory, Academy Sinica, Nanjing, China

ABSTRACT

Non-LTE calculations, with the non-thermal ionization effects included, indicated that for electron bombardment, the Hα line is widely broadened and shows a strong central reversal. Significant enhancements at the line wings of Lyα and Lyβ are also predicted at the beginning of the impulsive phase of flares. For the proton bombardment, no strong broadening and no large central reversal are expected. However, due to proton-hydrogen charge exchange, the enhancements at the red wings of Lyα and Lyβ lines at the early impulsive phase of flares are significant. Our results show that the electron beam can also in some cases generate visible and UV continuum emission in white-light flares. However, at the onset phase, a negative flare may appear within several seconds, due to the increase of the H^- opacity. Another spectroscopic signature of energetic particles, i.e. the impact polarization of atomic lines, is also mentioned.

I. INTRODUCTION

In solar flares, the non-thermal electrons of more than 10 KeV and protons of more than 1 MeV can be detected by their X-ray continuum and/or γ- ray line emission. However, non-thermal electrons and protons of energy as low as 100 KeV can be diagnosed by use of the UV and optical spectra of solar flares.

An important role of the non-thermal particle bombardment on the solar atmosphere is the non-thermal ionization and excitation (e.g. Chambe & Hénoux 1979; Aboudarham & Hénoux 1986; 1987). However, in most of previous semi-empirical modelling and dynamical simulations of solar flare atmospheres, this non-thermal effect has been either not included or underestimated. Another signature of proton bombardment can be found in the enhancement of the red wing of chromospheric lines, due to Doppler-shifted emission of the neutral hydrogen atoms formed by proton-hydrogen charge exchange (e.g. Canfield & Chang 1985).

In recent years, with correct estimates of the non-thermal excitation and ionization rates, we have calculated non-thermal hydrogen profiles and white-light continuum (Fang et al. 1993; Hénoux et al. 1993; Hénoux et al. 1995, thereafter referred to as Paper I, II and III respectively). Using more recent values of the atomic parameters and a refined atmospheric model, we have computed the non-thermal hydrogen line profiles resulting from the proton-hydrogen charge exchange (Fang et al. 1995). In this paper, we will give a brief review of our works. The impact polarization of atomic lines resulting from the particle bombardment on the flaring atmosphere has also been mentioned.

II. EFFECTS OF NON-THERMAL PARTICLE BEAMS

(a) Non-Thermal Excitation and Ionization Rates

A four-levels plus continuum atomic model of hydrogen was used. According to the theory given in Paper I and II, the non-thermal excitation and ionization rates of hydrogen by electron or proton beams can be obtained as

$$C_{12}^B \simeq 2.94\,10^{10}\frac{1}{n_1}\frac{dE^H}{dt}, C_{13}^B \simeq 5.35\,10^9\frac{1}{n_1}\frac{dE^H}{dt},$$
$$C_{14}^B \simeq 1.91\,10^9\frac{1}{n_1}\frac{dE^H}{dt}, C_{1c}^B \simeq 1.73\,10^{10}\frac{1}{n_1}\frac{dE^H}{dt},$$

where n_1 is the population at the ground level. dE^H/dt is the rate of energy deposit by an electron or proton beam. It is given by (Emslie 1978; Chambe & Hénoux 1979)

$$\frac{dE^H}{dt} = \frac{1}{2}(1-x)n_H\Lambda'\frac{K\mathcal{F}_1}{E_1^2}\left(\frac{N}{N_1}\right)^{-\frac{\delta}{2}}(\delta-2)\int_0^{u_1}\frac{u^{\frac{\delta}{2}-1}du}{(1-u)^{\frac{2+\overline{\beta}}{4+\beta}}}, \quad (1)$$

Where x is the ionization degree. The particle flux is supposed to be proportional to $E^{-\delta}$, with a low energy cut-off E_1. $\mathcal{F}_1$ is the total energy input flux above E_1. N_1 is the deepest column depth reached by the particles of energy E_1. A given column density N can only be reached by particles of energy greater than E_N. $E_N = [(2+\overline{\beta}/2)\overline{\gamma}\,K\,N/\mu_0]^{1/2}$, where μ_0 is the cosine of the angle between the initial velocity vector and the solar vertical; $K = 2\pi e^4$; $\overline{\beta}$ and $\overline{\gamma}$ are the mean values along the particle trajectory of β and γ, which are defined in Emslie's paper. The parameter u is defined as $u = (E_N/E)^2$, so that $u_1 = 1$ for $N > N_1$; $u_1 = N/N_1$ for $N \leq N_1$.

(b) Line Profile Diagnostics

The non-LTE numerical code is described in Paper I and II. That is, the non-thermal rates are included in the statistical equilibrium equations. Then, the statistical equilibrium equations and the transfer equations for

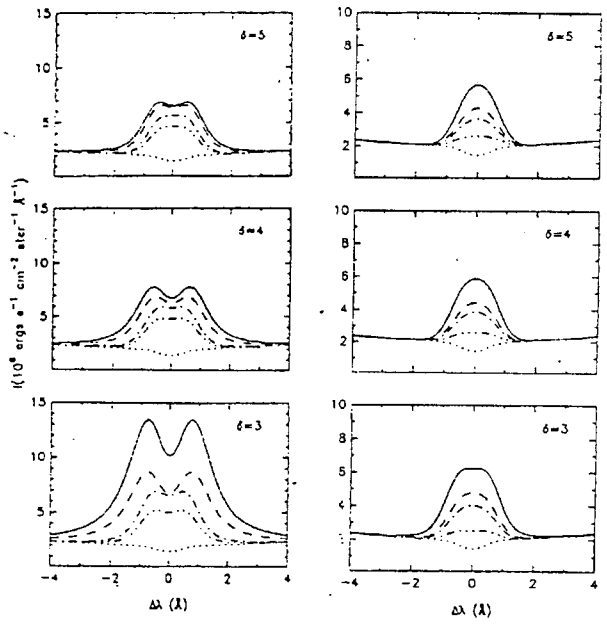

Fig. 1.— Hα line profiles for the model F_1 and for different values of δ. Left panel: the case of electron beam bombardment with $\mathcal{F}_1 = 1\ 10^{12}$(full line), $5\ 10^{11}$ (dashed line), $1\ 10^{11}$ (dash-dotted line) and $5\ 10^{10}$(line with three dots per dash) erg cm^{-2} s^{-1}. Right panel: the case of proton beam bombardment with $\mathcal{F}_1 = 5\ 10^{10}$ (full line), $1\ 10^{10}$ (dashed line), $5\ 10^{9}$ (dash-dotted line) and $1\ 10^{9}$ (line with three dots per dash) erg cm^{-2} s^{-1}. Dotted lines are for the same model but without including the non-thermal effects

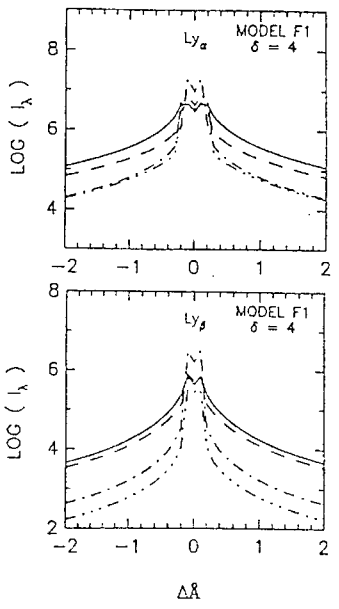

Fig. 2.— Lyα and Lyβ line profiles resulting from the bombardments on the F_1 model by electron (full lines) and proton (dotted-dashed lines) beams, assuming a particle acceleration site located at a coronal mass $m_0 = 0$. Dashed lines correspond to a coronal mass equal to $3.14\ 10^{-4}$ g cm^{-2}. An energy flux $\mathcal{F}_1 = 5\ 10^{11}$ erg cm^{-2} s^{-1} was adopted. The low-energy cutoff E_1 is taken to be 20 KeV for electron beam and 150 KeV for proton beam

hydrogen, coupled with the hydrostatic equilibrium and the particle conservation equations, have been solved iteratively. Five broadening mechanisms, i.e. the Doppler broadening, radiative damping, Van de Waas forces, linear and quadratic Stark effects, have been included in the calculations.

In order to show clearly the influence of the non-thermal effects on the hydrogen line intensities, we used the same temperature distributions given by the semi-empirical flare models of F_1 and F_2 (Machado et al. 1980). The non-thermal Hα, Lyα and Lyβ line profiles have been computed for various values of the total input energy flux $\mathcal{F}_1$ and the power index δ. Considering that the three lines are formed at the upper chromosphere, where $x \simeq 0.8 \sim 0.9$, so for an electron beam with an energy mainly of several tens of Kev, we can use the values of parameters as: $\Lambda' = 9$, $\overline{\beta} \simeq 2$, $\overline{\gamma} \simeq 15$, $E_1 = 20$ KeV. For a proton beam with energy of 100 Kev – 1 Mev, we adopted $\Lambda' = 4$, $\overline{\beta} \simeq 0$, $\overline{\gamma} \simeq 18 m_p/m_e$, $E_1 = 150$ KeV.

Figure 1 shows the Hα line profiles for the F_1 model with the different values of $\mathcal{F}_1$ and δ. Figure 2 gives the Lyα and Lyβ line profiles for the F_1 model. A power index $\delta = 4$, and an energy flux $\mathcal{F}_1 = 5\ 10^{11}$ erg cm^{-2} s^{-1} was adopted. It can be seen that the intensity enhancements of the Hα line and at the wings of Lyα and Lyβ lines caused by electron beam bombardment is much larger than that by proton beam, even for the same input energy flux $\mathcal{F}_1 = 5\ 10^{11}$ ergs cm^{-2} s^{-1}, which in fact is already too large for the proton beam. Figure 2 also indicates that the non-thermal effect is model-dependent: the intensity enhancement for the case of taking coronal mass $m_0 = 0$ is ~~the strongest~~ in ~~the Figure~~. ~~Thus~~, it is obvious that at the beginning of the impulsive phase of a flare, when the coronal mass is relatively low, the non-thermal effect should be most pronounced and can be detected, if the particle (especially electron) beam has adequate input energy. After the maximum of the impulsive phase, the non-thermal effect will decrease rapidly due to the steep increase of the coronal mass during the impulsive phase (e.g. Fang et al. 1986).

(c) Continuum Emission Diagnostics

For computing the continuum emission, the contributions from free-bound and free-free transitions for both hydrogen and H^-, as well as the Thomson scattering have been included in the non-LTE numerical code. The continuum contrast is defined as $R(\mu) = [I_f(\mu) - I_q(\mu)]/I_q(\mu)$, where $I_f(\mu)$ and $I_q(\mu)$ are continuum intensities for the flare and the preflare (quiet-Sun

model VAL-C by Vernazza et al. 1981) atmospheres, respectively. μ is the cosine of the heliocentric angle θ.

Figure 3 gives the results of R in dependence on $\mathcal{F}_1$ and μ for the case of electron bombardment. It can be seen that the electron beam will obviously increase the Balmer and Paschen continua (see also Aboudarham & Hénoux, 1986; 1987). The reason is that the rise of electron density due to non-thermal ionization leads to an increase of the recombination rates and to an increase of the populations at excited atomic levels. For proton bombardment, this effect is less pronounced, because the enhancement of the electron density is less than the case of electron bombardment (Paper II).

Figure 3 also shows that at $\lambda = 500$ nm, R is actually negative in regions near the solar disk center, resulting in a negative flare (Hénoux et al. 1992). It is mainly due to the enhanced H^- opacity in the lower atmosphere. After the heating of the lower atmosphere, R will become positive and then a white-light flare would appear.

III. EFFECT OF PROTON-HYDROGEN CHARGE EXCHANGE

We considered only the hydrogen line emission at the center of the solar disk that results from the bombardment of a vertical proton beam. Due to charge exchange between beam protons and ambient hydrogen atoms, a beam proton captures an electron from a target neutral hydrogen atom and becomes an energetic hydrogen atom excited to level j. The radiation of superthermal atoms is Doppler shifted and the line intensity enhancement is given by

$$\Delta I_{ji}(\Delta\lambda) = \frac{(2m_pE)^{1/2}c^2h}{4\pi\lambda_{ji}^2}\int_0^\infty n_j(E,z)A_{ji}dz, \quad (2)$$

where $n_j(E,z)$ is the number density of the superthermal particles of energy E excited to the level j in (E,z)-phase space. A_{ji} is the spontaneous transition rate. Giving an atmospheric model and the parameters of a proton beam ($\delta, \mathcal{F}_1$, E_1), we can solve the statistical equilibrium equation and the conservation equation of the non-thermal protons, and then obtain the line intensity. The details can be found in the paper of Fang et al. (1995).

Using more recent values of atomic parameters and the semi-empirical flare model F_1 , we have computed the Hα, Lyα and Lyβ line profiles for different parameters of δ , E_1 and $\mathcal{F}_1$. Figure 4 gives the results. It can be seen that the non-thermal enhancement should be detectable in the red wings of Lyα and Lyβ lines. Our study shows that the emission will be the highest at the early stage of the impulsive phase, when the coronal mass is low. The Hα non-thermal emission was found too small to be detectable.

IV. IMPACT POLARIZATION DIAGNOSTICS

Recent observations showed that a linear polarization degree as high as 2.5% – 5% is detected in the Hα line of solar flares within some Hα-bright patches (e.g. Hénoux et al. 1990). The electric vector is radial. The most probable cause of this polarization is proton beam impact on neutral hydrogen in flaring loops, with a dominant effect at their feet (Hénoux et al. 1990). A neutral beam carrying protons and electrons with equal velocities would be even more efficient. Local anisotropies of the cold chromospheric protons associated to current closure during electron bombardment could also lead to radial linear polarization (Emslie & Hénoux 1995). Electron beam may produce tangential line linear polarization (Firstova & Boulatov 1995).

In summary, it is possible to diagnose energetic particles of solar flares by use of the UV and optical spectroscopy.

ACKNOWLEDGEMENTS

This work was partly supported by a key project from the National Science Committee and the National Science Foundation of P.R. China.

REFERENCES

Aboudarham, J., & Hénoux, J. C. 1986, A&A, 156, 73

Aboudarham, J., & Hénoux, J. C. 1987, A&A, 174, 270

Canfield, R. C., & Chang, C. R. 1985, ApJ, 295, 275

Chambe, G., & Hénoux, J. C. 1979, A&A, 80, 123

Ding, M. D., & Fang, C. 1996, A&A, in press

Emslie, A. G. 1978, ApJ, 224, 241

Emslie, A.G., & Hénoux, J. C. 1995, in Pulkovo Workshop on Solar Polarization, in press

Fang, C., Feautrier, N., & Hénoux, J. C. 1995, A&A, 297, 854

Fang, C, Huang, Y.R, Hu, J., & Gan, W.Q. 1986, in D.Neidig (ed.), The Lower Atmosphere of Solar Flares, NSO, Sunspot, NM. p.117

Fang, C., Hénoux, J. C., & Gan, W. Q. 1993, A&A, 274, 917 (Paper I)

Firstova, N. M., & Boulatov, A. V. 1995, in Pulkovo Workshop on Solar Polarization, in press

Hénoux, J.C., & Aboudarham, J. 1992, In: Svestka Z., Jackson B.V., Machado M.E. (eds) Eruptive Solar Flares, Springer-Verlag, p.118

Hénoux, J. C. et al., 1990, ApJ, 73, 303

Hénoux, J. C., Fang, C., & Gan, W. Q. 1993, A&A, 274, 923 (PaperII)

Hénoux, J. C., Fang, C., &Gan, W. Q. A&A, 297, 574 (PaperIII)

Machado, M. E., Avrett, E. H., Vernazza, J. E., & Noyes, R. W. 1980, ApJ, 242, 336

Vernazza, J. E., Avrett, E. H., & Loeser, R. 1981, ApJS, 45, 635

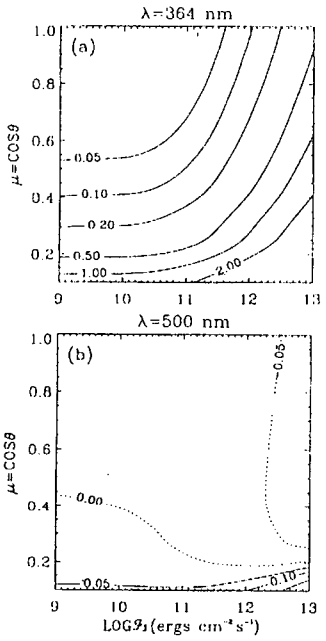

Fig. 3.— Contours of the continuum contrast R with respect to different values of $\mathcal{F}_1$ and μ, for **a** λ = 364 nm and **b** λ = 500 nm . The electron beam is assumed to have a power index $\delta = 4$ and a cut-off energy $E_1 = 20$ KeV (Ding & Fang, 1996)

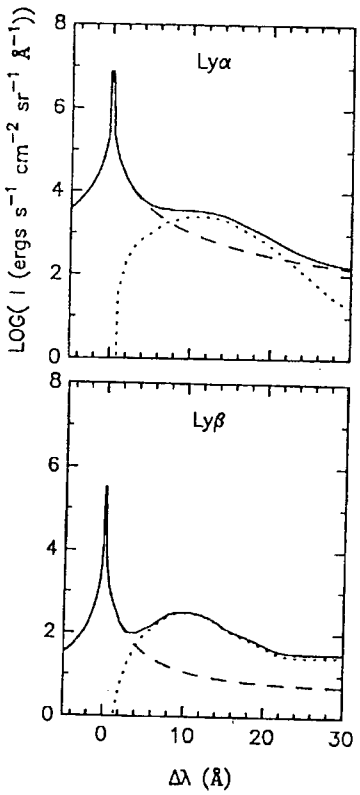

Fig. 4.— The total Lyα and Lyβ line profiles (full line) as the sum of the profiles emitted by the background atmosphere (dashed line) and of the non-thermal spectral emission (dotted line) generated by a proton beam with δ = and $\mathcal{F}_1 = 5\ 10^{10}$ erg cm^{-2} s^{-1} above a energy cutoff E = 150 KeV. Both are calculated for the semi-empirical flar model F_1.